ORIGINAL RESEARCH

Treatment of natural mammary gland tumors in canines and felines using gold nanorods-assisted plasmonic photothermal therapy to induce tumor apoptosis

Moustafa R K Ali[1]
Ibrahim M Ibrahim[2,†]
Hala R Ali[2,3]
Salah A Selim[2]
Mostafa A El-Sayed[1,4]

[1]School of Chemistry and Biochemistry, Georgia Institute of Technology, and Laser Dynamics Laboratory, Atlanta, GA, USA;
[2]Department of Veterinary Medicine, Cairo University, Giza, Cairo, Egypt;
[3]Department of Bacteriology and Immunology, Animal Health Research Institute (AHRI), Dokki, Giza, Egypt;
[4]School of Chemistry, King Abdul Aziz University, Jeddah, Saudi Arabia

†Ibrahim M Ibrahim passed away on August 23, 2015

Correspondence: Mostafa A El-Sayed
School of Chemistry and Biochemistry, Georgia Institute of Technology, and Laser Dynamics Laboratory, 901 Atlantic Drive, Atlanta, GA 303320400, USA
Email melsayed@gatech.edu

Salah A Selim
Department of Veterinary Medicine, Cairo University, Giza square, Cairo, 12211, Egypt
Email dr.salahselim@hotmail.com

Abstract: Plasmonic photothermal therapy (PPTT) is a cancer therapy in which gold nanorods are injected at the site of a tumor before near-infrared light is transiently applied to the tumor causing localized cell death. Previously, PPTT studies have been carried out on xenograft mice models. Herein, we report a study showing the feasibility of PPTT as applied to natural tumors in the mammary glands of dogs and cats, which more realistically represent their human equivalents at the molecular level. We optimized a regime of three low PPTT doses at 2-week intervals that ablated tumors mainly via apoptosis in 13 natural mammary gland tumors from seven animals. Histopathology, X-ray, blood profiles, and comprehensive examinations were used for both the diagnosis and the evaluation of tumor statuses before and after treatment. Histopathology results showed an obvious reduction in the cancer grade shortly after the first treatment and a complete regression after the third treatment. Blood tests showed no obvious change in liver and kidney functions. Similarly, X-ray diffraction showed no metastasis after 1 year of treatment. In conclusion, our study suggests the feasibility of applying the gold nanorods-PPTT on natural tumors in dogs and cats without any relapse or toxicity effects after 1 year of treatment.

Keywords: gold nanorods, natural mammary tumors, plasmonic photothermal therapy, canine, feline

Introduction

Plasmonic nanoparticles (NPs) exhibit unique physical and chemical properties that can be utilized for both cancer treatment and diagnosis. In plasmonic photothermal therapy (PPTT), NPs such as gold nanorods (AuNRs) absorb near-infrared (NIR) light resulting in hyperthermia, thereby inducing tumor ablation. In PPTT, cancer cells show a much higher uptake of NPs than normal cells.[1] Although many traditional cancer therapies with drugs or radiation cause side effects due to their toxicity to normal cells, PPTT has fewer side effects mainly because of its selectivity to cancer cells. In PPTT, two selective targeting methods can be applied: 1) active targeting and 2) passive targeting. In active targeting, specific surface modifications (ligands) of NPs can recognize and bind to the receptors on the surface of cancer cells. On the other hand, in passive targeting, NPs are usually injected directly to solid tumor and accumulate inside the tumor mainly via the enhanced permeability and retention effect. The enhanced permeability and retention effect has been regarded as a primary rationale for the delivery of NPs due to the leaky tumor blood vasculature. Then, the

tumor will be irradiated with laser, causing localized heat for killing cancer cells.[2–6] These attributes of PPTT make it a superior alternative in cancer treatment.

Among all plasmonic gold NPs, three types have shown the greatest potential for use in cancer PPTT: gold nanocages, gold nanoshells (AuNSs), and AuNRs.[7–9] These three types of NPs have been synthesized with specific sizes and shapes designed to enable absorption of NIR radiation and allow for subsequent heat transmission. Due to the toxicological properties that could result from the presence of unused silver (Ag) on the interior of the nanocage during its synthesis, the widespread use of gold nanocages for the treatment of cancer is not likely to occur.[10] The AuNSs plasmon wavelength is dependent on the ratio of the thickness of the shell to the core diameter.[1] Thus far, the use of AuNSs has been limited to the US Food and Drug Administration-approved use of the AuNSs AuroLase® (Nanospectra Biosciences, Inc., Houston, TX, USA) for PPTT clinical trials of head and neck cancer.[1] One challenge of using AuNSs is the difficulty of synthesizing them with a uniform ratio of shell to core radii. AuNRs exhibit a longitudinal NIR surface plasmon resonance band that is directly proportional to its aspect ratio (length/width). Among all plasmonic gold NPs, AuNRs are regarded as one of the most feasible options for absorbing NIR laser radiation.[11–14] For example, a recent publication compared the efficacy of AuNRs with that of AuNSs and found that AuNRs intrinsically have greater absorption efficacy per gram of gold and longer circulation half-life in vivo.[15] Additionally, PPTT-AuNRs studies have shown encouraging results with no significant toxicological side effects in vivo (xenograft mice model).[16–19]

PPTT can induce cell death primarily by two pathways: necrosis and apoptosis.[20] During necrosis, the heat induced from PPTT disrupts the plasma membrane causing the cytoplasmic components to leak out and inflammation to occur within the cell. However, apoptosis is a highly regulated cell death pathway and would thus be a cleaner way for eliminating cancer cells. Therefore, modulating PPTT to trigger apoptosis would be more favorable in clinical studies. It has been reported that different intracellular locations or shapes of NPs regulate the switch between necrosis and apoptosis.[21,22] In this study, we were able to cause cancer cell apoptosis in vitro and in vivo by adjusting the laser exposure time.

The primary novelty of this study was the extension of AuNRs-assisted PPTT to natural tumors in animals larger than ones used in any previous study. Mammary gland tumors of epithelial origin are very common neoplasms of canines and felines. The similarity of molecular and biological machinery of canines/felines and that of humans suggests the suitability of using mammary tumors of these animals as a model for the study of human mammary tumors.[23–25] The second novelty was the optimization of AuNRs-PPTT's conditions to generate tumor apoptosis as a favorable cell death mechanism (rather than necrosis).[12,26,27] Herein, we directly injected the PEGylated AuNRs to the mammary tumors of each canine/feline as opposed to intravenous injection, as our previous study showed a better efficacy for intratumoral injection than intravenous injection,[1] although the latter could be helpful for some applications (especially for tumors that are not accessible for direct injection of AuNR).[8] We tested PPTT on canine and feline natural mammary gland tumors. To minimize side effects, we optimized PPTT dosages to enable a slow cancer cell apoptosis. Using our optimized protocol, adjusting the photothermal temperature to 44°C, we were able to ablate 100% of tumors in seven animals without any relapse or toxicity effect after 1 year from the tumor treatment.

Materials and methods
Synthesis and surface modification of AuNRs

AuNRs were prepared according to the literature.[28] Briefly, $HAuCl_4$ (5 mL, 1 mM; Sigma-Aldrich, St Louis, MO, USA) was added to 5 mL of cetyltrimethylammonium bromide (CTAB, 0.20 M; Sigma-Aldrich). $AgNO_3$ (250 µL, 4 mM; Sigma-Aldrich) was then added and the pH of the solution adjusted to 1–1.15. Around 70 µL of ascorbic acid (78.8 mM; Sigma-Aldrich) was added to the solution until the solution became clear. Ice-cold $NaBH_4$ (15 µL, 0.01 M; Sigma-Aldrich) was injected into the unstirred growth solution immediately and then allowed to react for 6 hours. The resulting AuNRs had dimensions of approximately 25×5 nm (see "Formulation and characterization of the AuNRs" section, Figure 1). AuNRs were concentrated by centrifuging at 19,745 rcf for 15 minutes. The pellet was redispersed in water and centrifuged at 19,745 rcf for an additional 15 minutes. Then methoxy polyethylene glycol (PEG) thiol (m-PEG-Th, PEG; Laysan Bio, Arab, AL, USA) was added to the CTAB-conjugated AuNRs and was incubated overnight in a shaker. A final ratio of about 20,000 PEG molecules per NP was achieved after centrifugation to remove unconjugated PEG.

Characterization of AuNRs

The characterization of AuNRs was carried out using a Cary 500 UV–Vis Spectrometer (Agilent Technologies, Santa
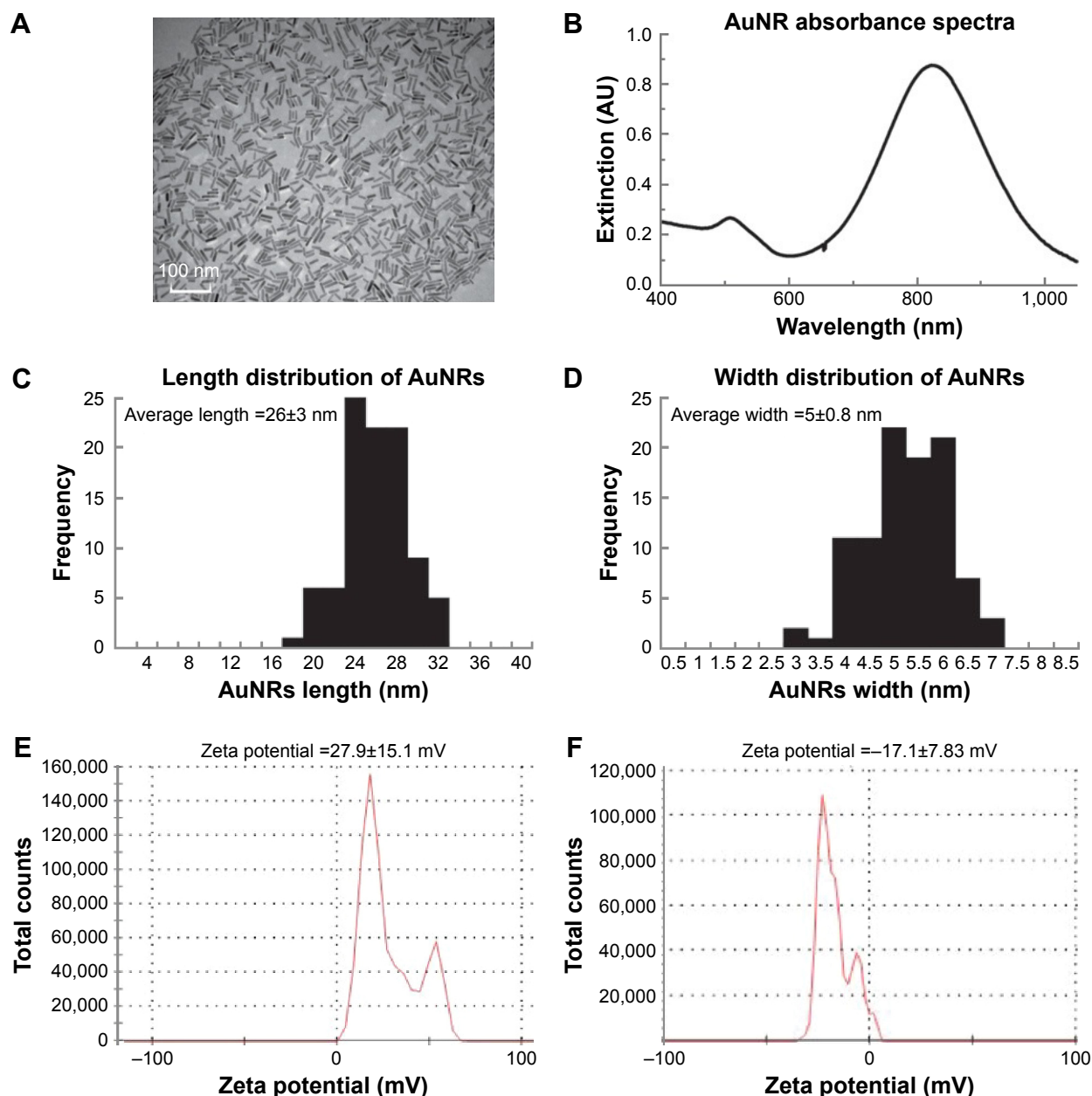
A

B

C

D

E

F

Figure 1 Characterization of PEGylated AuNRs (length 26±3 nm, width 5±0.8 nm).
Notes: (**A**) TEM image with 100 nm scale bar. (**B**) UV–Vis absorbance spectra showing the SPR peaks of AuNRs. (**C**) Corresponding histograms of the lengths of the 100 AuNRs particles counted. (**D**) Corresponding histograms of the widths of the 100 AuNRs particles counted. (**E**) Zeta potential data of the as-synthesized rods. (**F**) Zeta potential data of PEGylated AuNRs.
Abbreviations: AuNRs, gold nanorods; TEM, transmission electron microscope; SPR, surface plasmon resonance; UV–Vis, ulltraviolet–visible.

Clara, CA, USA) for the spectroscopic measurements, and a JEOL 100 CX transmission electron microscope (TEM) (JEOL Ltd., Tokyo, Japan) was used to image the samples. Zeta potentials were measured using a ZetaSizer 3000 HAS (Malvern Instruments, Worcestershire, UK). Zeta potential was tested to characterize the surface conjugation with PEG. Ellman's reagents (react with free-SH group; Sigma-Aldrich) were used to quantify the number of PEG molecules bound to the surface of the AuNRs.[29] Ellman's

reagent reacts with free-SH group and can be measured calorimetrically at 412 nm. By subtracting the absorbance of the residual PEG, in the supernatant solution after PEG conjugation and centrifugation, from the original absorbance of the solution before adding to AuNRs, we can calculate the number of PEG molecules on the surface of AuNRs by Beer's law. The results of characterization are described below (see "Formulation and characterization of the AuNRs" section).

Animal diagnosis, ultrasonography, and X-ray examination

The animals were admitted to the clinic of Department of Surgery, Faculty of Veterinary Medicine, Cairo University. All pets' owners claimed that their animals did not receive any treatment before their arrival at the university. Histopathology tests were used to diagnose the tumors as adenocarcinoma without any skin invasion, except for one tumor (Case 1, Tumor 6). Seven animals were included in this study, five canines (females) and two felines (females), and the total number of tumors was 13. All animals were handled in accordance with Association for Assessment and Accreditation of Laboratory Animal Care and Office of Laboratory Animal Welfare guidelines under the direction of the Institutional Animal Care and Use Committee. All animal experiments were approved by the Experimental Animal Ethical Committee Faculty of Veterinary Medicine, Cairo University. The animal experiments were carried out after owner permission and a high standard of veterinary care was involved. Ultrasonography examination was performed with a real-time Toshiba medical company ultrasound system (Toshiba, Tokyo, Japan), using multifrequency probes (7 microns convex and 7 MHz linear probe) with displayed depth of 4–6 mm. The scans and photographs were taken on Polaroid in both longitudinal and transverse scans. At the tumor site, the animal's hair was clipped and shaved, and subsequently, sonographic gel was applied to the skin of the animals. Radiographic recordings were taken with an X-ray machine (Fischer, Berlin, Germany). The radiographic setting factors were 58 to 70 kVp, 10 mAs, and 90 cm focal spot–film distance. The radiographic exposures were conducted, dorsoventrally and right laterally. The tumor dimensions were measured using calipers and confirmed with sonar.

Performing PPTT in animals

Each animal was subjected to three sessions of PPTT treatment in 2-week intervals using an 808 nm diode laser with a power of 5.8 W/cm^2 and a spot size of around 5.6 mm^2. An effective dose of AuNRs solution (7.5 nM AuNRs) for each 100 cm^3 was used, and the amount used was scaled up based on the volume of the tumor and injected directly into the tumor. Five minutes after injection, the entirety of the tumor was irradiated with the laser. The AuNRs concentration was decreased by 50% for each subsequent treatment. The temperature increase of a tumor during the laser irradiation was measured by placing a 33-gauge hypodermic thermocouple (OMEGA Engineering, Inc., Stamford, CT, USA) needle directly inside the tumor (42°C–44°C). The results of PPTT in animals, histopathology evaluation (see "Histopathology

evaluation for animals" section), blood analysis (see "Blood analysis" section), X-ray (see "Animal diagnosis, ultrasonography, and X-ray examination" section) are discussed in "Applying PPTT to animals" and "The physiological status of animals after 1 year from treatment" sections.

Histopathology evaluation for animals

The detailed pathologic evaluation of tumors was conducted by the members of the pathology department, Faculty of Veterinary Medicine, Cairo University. Histopathological analysis was performed on 5 µm sections from tumor tissue that were fixed in 10% buffered formalin. The samples were stained with hematoxylin and eosin to assess pathology.

Blood analysis

Blood analyses tests for examining the liver and kidney functions of the animals were conducted before and after treatment. The tests were performed according to the manufacturer's instructions using diagnostic kits of the StatLab Spectrum Diagnostics in Egypt. Absorption spectrometry with six light-emitting diodes as optical light source was used. The kits were purchased from Egyptian Company for Biotechnology (Obour city industrial area, Egypt).

Cell culture and PPTT optimization in vitro and in vivo

To examine the in vitro efficacy of PPTT and optimize the treatment condition (see "Optimization of PPTT toward generating cancer cell apoptosis" section), MCF-7 breast cancer cells (human adenocarcinoma; American Type Culture Collection, Manassas, VA, USA) were cultured in Dulbecco's Modified Eagle's Medium (Corning Incorporated, Corning, NY, USA) supplemented with 10% v/v fetal bovine serum, 1% penicillin/streptomycin at 37°C in a 5% CO$_2$ humidified atmosphere. For incubation, the growth media was removed from the cell cultures that had NPs and replaced with identical media containing PEGylated AuNRs (2.5 nM) overnight, and an 808 nm diode laser (power: 5.8 W/cm^2; spot size around 5.6 mm) was used on the cells. The level of cell ablation was related to the time of PPTT. Two time scales were used: 2 and 5 minutes.

For optimizing the PPTT condition in vivo, we applied PEGylated AuNRs (2.5 nM) for two different time periods (2 and 5 minutes) using an 808 nm diode laser (power: 5.8 W/cm^2; spot size around 5.6 mm). The result of optimization is shown in Supplementary materials.

Apoptosis/necrosis assay in vitro

MCF-7 cells (human breast cancer cells) were washed with phosphate-buffered saline and then trypsinized (Clonetech,

Mountain View, CA, USA).[29] After trypsinization, cells were centrifuged and washed with phosphate-buffered saline. Cells were then resuspended in 493 μL 1× annexin binding buffer (Invitrogen, Thermo Fisher Scientific, Waltham, MA, USA) with 2 μL working propidium iodide (PI; BioLegend, San Diego, CA, USA) 100 μg/mL and 5 μL annexin-V–fluorescein isothiocyanate (BioLegend) and then incubated at room temperature for 15 minutes. Subsequently, cells were filtered and subjected to flow cytometry using a BSR LSR II flow cytometer (BD Biosciences, San Jose, CA, USA). Samples were excited with a 488 nm laser, and fluorescein isothiocyanate was detected in FL-1 by a 525/30 BP filter, whereas PI was detected in FL-2 by a 575/30 BP filter. FlowJo software (Tree Star Inc., Ashland, OR, USA) was used to count annexin-V+ cells from at least 10,000 events.

Results

Formulation and characterization of the AuNRs

Based on our previous study in vitro, AuNRs with average length × width (26×5 nm) showed enhanced efficacy of PPTT, which was driven from the high ratio of the absorbed light to scattered light,[30–32] we synthesized AuNRs with similar dimensions using our reported method,[28] and these AuNRs are shown in the TEM image (Figure 1A). To absorb the near-IR laser light for performing PPTT, AuNRs were generated with an aspect ratio of about 5 and with a surface plasmon resonance wavelength of ~800 nm (Figure 1B). The approximate length and width were 26±3 nm and 5±0.8 nm, respectively, which was obtained by counting the length and width distributions of 100 particles (Figure 1C and D). After synthesis, AuNRs were successfully coated with mPEG-Th as shown by their zeta potential of −17.1±7.83 mV (Figure 1F), while as-synthesized AuNRs had a positive zeta potential (Figure 1E) because of positively charged CTAB. The number of PEG molecules per particle was observed to be approximately 20,000 PEG/AuNR.

Optimization of PPTT toward inducing cancer cell apoptosis

We developed a mild PPTT strategy that induced cell apoptosis using a reduced laser exposure time. We conducted PPTT in vitro (MCF-7 cells) and in vivo (mammary gland tumor) by irradiating the tumors for 2 or 5 minutes. The control sample that incubated with AuNRs but without laser treatment were shown in Figure S1A and B. After 2 minutes of laser irradiation, 42.7% and 2.89% of the population underwent apoptosis or necrosis, respectively (Figure S1C), whereas 5 minutes of

laser irradiation caused 20.17% and 15.5% of apoptosis or necrosis, respectively. The data demonstrates that a 5-minute irradiation time predominantly leads to necrosis (heating up to about 52°C), while on the other hand, a 2-minute irradiation time mainly results in apoptosis (Figure S1D, heating up to 42°C–44°C). This result is very comparable with the former study which showed that a low dose of heat induces apoptosis, whereas a high dose (heating above 50°C) induces necrosis.[21] For thermal damage of cells, Sapareto et al[33] proposed "cumulative equivalent minutes at 43°C (CEM43) apop" as a method to calculate the thermal dose applied. Using their methods, we calculated that the CEM43 of 5-minute irradiation is more than 500 times that of 2-minute irradiation. When laser was applied without AuNRs injection, no obvious temperature increase was observed.

Then, we used a preliminary optimal laser time on a single mammary gland tumor in a dog. We applied PPTT with two different irradiation times (2 and 5 minutes) to both sides of a single tumor. It was concluded that 2 minutes of irradiation caused a gentle change within the tumor, whereas 5 minutes of irradiation caused a very severe burning (Figure S1E). We related our thermal dosage to the average temperature that arose from the animal or cells after a 2-minute irradiation. In both cases, the temperatures are similar (42°C–44°C). Based on these preliminary experiments, we selected the 2-minute irradiation time as the optimal irradiation time for complete tumor treatment for all tumor groups.

Applying PPTT to animals

After establishing the dosage of an effective laser application time, the PPTT optimized conditions were conducted multiple times (0, 2, and 4 weeks) and tumor volumes evaluated every 2 weeks until complete regression, as shown in Figure 2. Before any PPTT treatment, tumors of all the animals showed variant growth, and after PPTT, obvious tumor regression was observed. All 13 tumors with variant volumes regressed with an average half-life of about 2 weeks and completely disappeared within 6–8 weeks. Images of tumor change and relevant histopathology in Case 7 (feline) show the tumor regression process (Tumor 6: open tumor and Tumor 10: close tumor). Although both tumors have different malignancy stages (Table 1), the images indicate that both tumors respond positively to the treatment, and no tissue burning was seen after gentle treatments. Histopathological examinations were carried out on tumors to investigate the malignancy of the tumors before and after PPTT. Photographic images (Figure 3), and also complete images of the case (Figure S2), showed the tumor statuses before, during, and after treatments. As shown in Figure 3A,
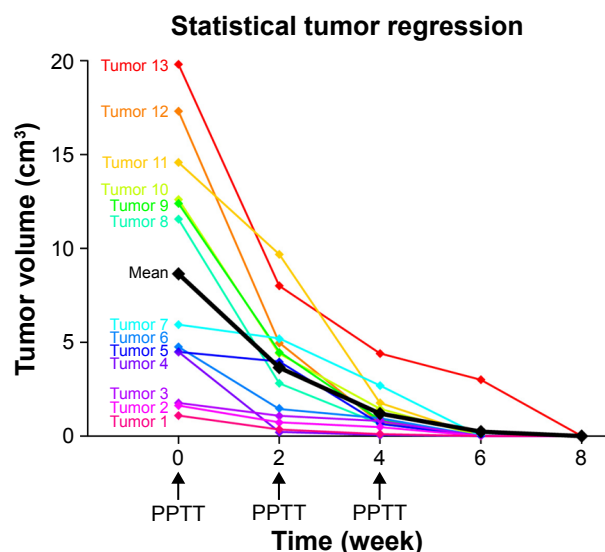
Statistical tumor regression

Figure 2 Regression curves of 13 tumors of variable volumes from multiple PPTT treatment (labeled with "arrow").
Note: The mean of the regression ("black line") shows the general efficacy of the treatment.
Abbreviation: PPTT, plasmonic photothermal therapy.

before treatment, Case 7 (Tumor 6) was diagnosed with well-differentiated and highly malignant adenocarcinoma according to histopathology. Figure 3A showed that the cells were arranged either in tubular pattern or solid masses, in which the acini were arranged in groups and surrounded by fibrous connective tissue stroma. The stroma was infiltrated with inflammatory cells, mainly macrophages and lymphocytes. The acini were lined by secretory cells without a basement membrane, and the nucleus appeared to be deeply basophilic with an enlarged, clear nucleolus. Poorly undifferentiated neoplastic mass characterized by a cluster of neoplastic cells with deeply basophilic cytoplasm and a vesiculated nucleus was observed. The tumor mass appeared highly cellular with low fibrous connective tissue stroma and loss of Grade IV acinar pattern (solid carcinoma).

Two weeks after the second treatment and before the third treatment, histopathology showed absence of epithelial lining of acini and basement membrane, indicating a decrease in malignancy. Also, it revealed the atrophy of acini with dense fibrous connective tissue proliferation. The mammary lobule appeared as involution stage Grade I (Figure 3B). Finally, after the third treatment, there was complete regression of the tumors. Additionally, 1 year after the third treatment, no relapses were observed for Case 7 (feline) (Figure 3C and E).

Furthermore, in Case 2 (canine), X-ray image showed there was no metastasis in the internal organs, and ultrasound image showed the tumor location, shape, and dimensions (Figure S3). Tumor statuses before, during, or after

Table I Blood profile for each case before treatment and 1 year after cure

Case no	Animal species	Age/year	Tumor location	Tumor size/grade	Urea (mg/dL) Before	Urea After 1 year	Urea Normal range	Creatinine (mg/dL) Before	Creatinine After 1 year	Creatinine Normal range	ALT (U/L) Before	ALT After 1 year	ALT Normal range	AST (U/L) Before	AST After 1 year	AST Normal range
1	Dog Griffon	10	12-left anterior thoracic	T3/VI	15	14.9	5–25	0.82	0.71	0.5–1.6	84	88	5–107	156	135	5–55
2	Dog Griffon	11	9-right abdominal	T3/III	28	34	5–25	0.87	0.91	0.5–1.6	49	84.4	5–107	84	61	5–55
			4-left caudothoracic	T1/III												
3	Dog Griffon	7	13-right abdominal	T3/III	26	24.2	5–25	1.6	1.1	0.5–1.6	115	117	5–107	142	123	5–55
			2-left caudothoracic	T1/III												
4	Dog Griffon	5	8-right cranioinguinal	T3/III	27	26.8	5–25	0.96	0.85	0.5–1.6	72	76	5–107	140	96	5–55
5	Dog Griffon	13.5	7-left cranioinguinal	T3/VI	15	20	5–25	1.2	1.1	0.5–1.6	76	88	5–107	35	42	5–55
			5-left cranioinguinal	T2/VI												
			3-left inguinal lymph node	T3/III												
6	Cat Shirazi	11	11-right caudoinguinal	T2/III	38.7	35.6	14–36	1.6	1.4	0.6–2.4	56.2	58.4	10–100	34.5	36.2	10–100
			1-left craniothoracic	T1/III												
7	Cat Shirazi	4	6-left anterior thoracic	T2/IV	26.4	24.9	14–36	1.8	1.3	0.6–2.4	19	25	10–100	16	14	10–100
			10-right post-caudoinguinal	T3/IV												

Abbreviations: ALT, alanine transaminase; AST, aspartate transaminase.
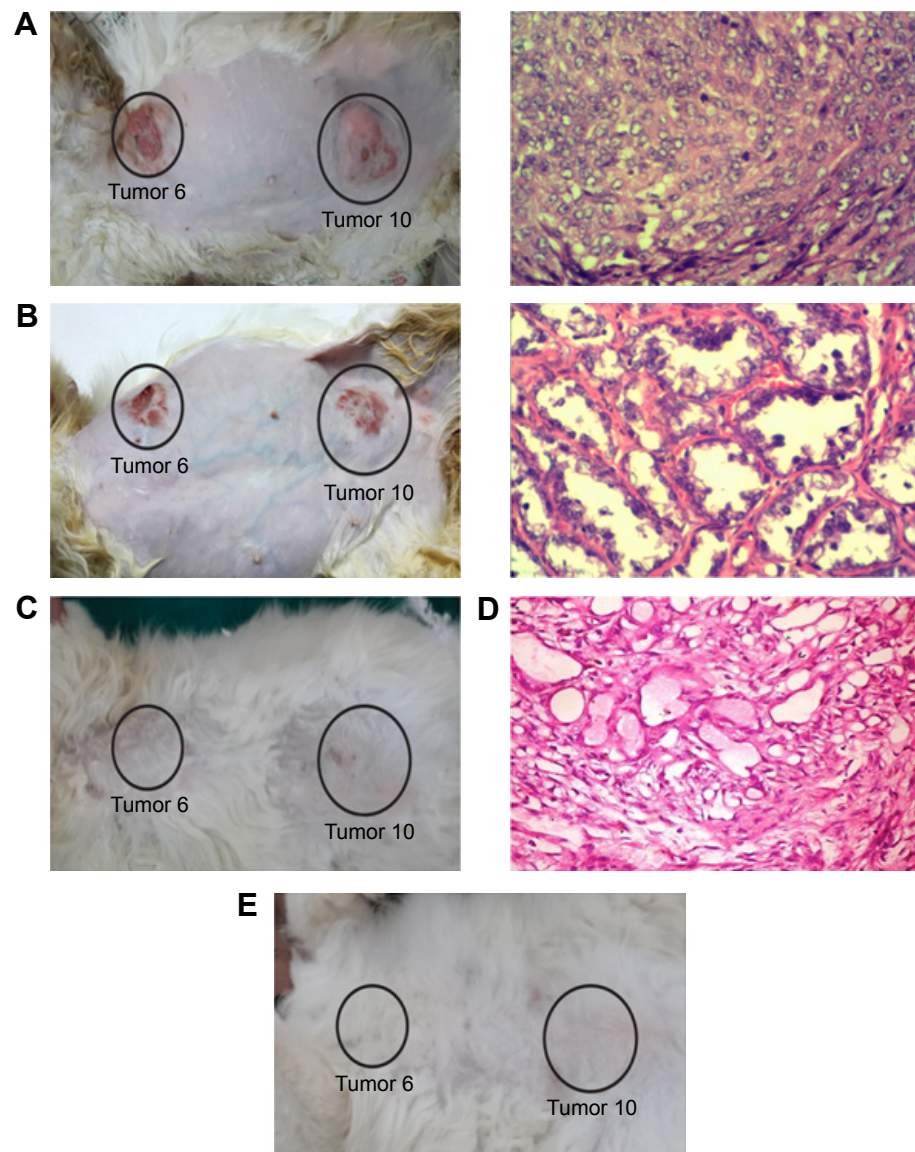
Figure 3 Photographs for Case 7 (feline) with two tumors (Tumor 6: anterior thoracic opened tumor; and Tumor 10: caudoinguinal tumors) and histopathology images (Tumor 6) showing the tumor regression before and/or after each treatment.
Notes: (**A**) Before first treatment, (**B**) before second treatment, (**C**) after third treatment, (**D**) before third treatment, and (**E**) 1 year after third treatment, no relapse is observed. After 1 year, the tumors completely disappeared, thus we were unable to take histopathology data for the animals. Magnification of histopathology images stained with H&E: (**A**) and (**D**) ×100; (**B**) ×200.
Abbreviation: H&E, hematoxylin and eosin.

treatments are seen in Figure 4, and other photographs for Case 2 are shown in Figure S4. For the tissue sections, moderately undifferentiated tumor mass characterized by basophilic cells with condensed nuclear chromatin lining the acini are observed (Figure 4A). The connective tissue stroma was infiltrated with mononuclear cells of mainly lymphocyte and macrophage origin but also contained some multinucleated giant tumor cells (Grade III). On the other hand, after treatment (Figure 4B) histopathology revealed some necrosis of acini accompanied with cellular stroma (Grade 0). No metastasis was observed based on X-ray

diffraction images (Figure 5). Similarly, Case 3 has been explained in the Supplementary materials, along with photographic images taken before treatment, 2 weeks after treatment, and 1 year after treatment (Figure S5, photographs). Histopathology images for Case 3 before treatment shows the tumor grade change from Grade III before treatment to Grade 0 after the treatment (Figure S6). Furthermore, the X-ray images before and after treatment show there is no metastasis in both statuses (Figure S7).

Images of tumor change and relevant histopathology in Case 7 (feline) show the tumor regression process (Tumor 6:
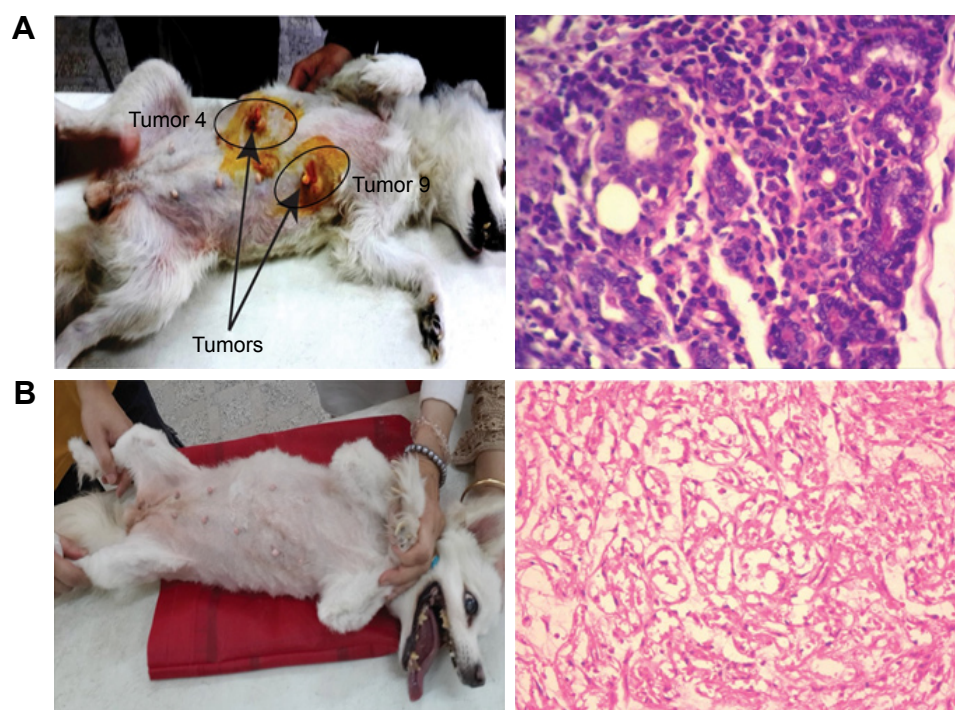
Figure 4 Photographs for Case 2 (canine; Tumor 4: left caudothoracic and Tumor 9: right abdominal mammary gland) and histopathology images (Tumor 4) showing the tumor status before treatment (**A**) and 2 weeks after third treatment (**B**).
Note: Magnification of histopathology images stained with H&E: ×100.
Abbreviation: H&E, hematoxylin and eosin.

open tumor and Tumor 10: close tumor). Although both tumors have different malignancy stages (Table 1), the images indicate that both tumors responded positively to the treatment, and no tissue burning appeared after the gentle treatments. The regression curve as shown in Figure 2 shows a dramatic tumor regression with normal hair growth. Furthermore, 1 year after the completion of treatment, no subject exhibited signs of relapse or effects of toxicity, and even the hair grew back naturally.

The physiological status of animals after 1 year from treatment

Short-term toxicity of AuNRs-PPTT was regarded as minimal because of the normal behavior and the animal's activity, diet, body weight, and appearance. In addition, the study of AuNRs toxicity on mice models has proved its short-term safety.[15,20] For long-term safety, a complete blood profile picture for all the cases was examined at two different times: once before the treatment and once 1 year after treatment. The objective was to follow-up the animals 1 year after their final treatment and check for any changes in anatomical function (liver and kidney) as well as their overall health (eg, body weight, physical activity, and body skin). No significant change was observed in liver (alanine

transaminase and aspartate transaminase) and kidney (urea and creatinine) functions when comparing before treatment and 1 year after treatment, although some animals did have abnormal initial blood analysis results before treatment, which might be due to their different health or diet conditions (Table 1). In summary, this result suggests no obvious change in liver and kidney functions and that PPTT is safe even after 1 year.

Discussion

Our data suggests that administering AuNRs in conjunction with very low photothermal conditions of 42°C–44°C for 2 minutes to canines and felines with natural tumors triggers apoptosis, which is more favorable for tumor treatment than necrosis. We tracked the animals after treatment for 1 year and found no tumor relapse or metastasis, or any negative physiological changes, indicating that there is no toxicity when using optimized AuNRs-PPTT conditions. We did not observe changes in liver and kidney function 1 year after treatment. In addition, the normal behavior and animal's activity, diet, body weight, and appearance indicate no biotoxicity of AuNRs. To our knowledge, this is the first study supporting the efficacy and safety of AuNRs-PPTT applied to natural mammary tumors in canines and felines.
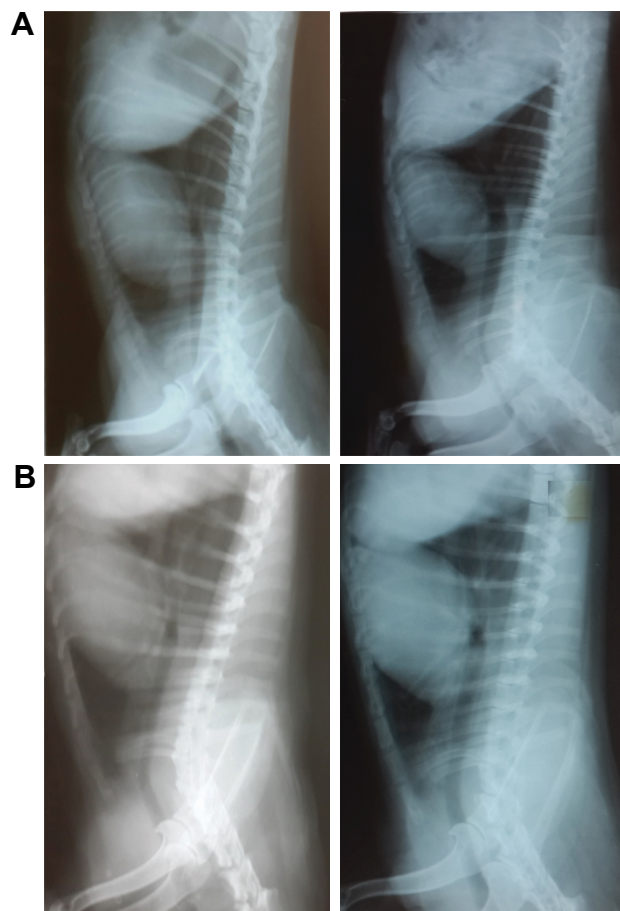
Figure 5 X-ray lateral exposure for Case 7 (feline) (**A**) and Case 2 (canine) (**B**).
Notes: Left: 2 weeks after third treatment and right: 1 year after third treatment showing that there is no metastasis.

A previous study has reported that AuNRs-PPTT can induce cell apoptosis following the common mitochondrial alternative pathway, reactive oxygen species production, Ca^{2+} release, mitochondrial membrane potential change, cytochrome C release, and the subsequent activation of the caspase family.[34–38] Besides this, other potential mechanisms of PPTT-induced apoptosis have been reported, such as initiating Golgi apparatus–endoplasmic reticulum dysfunction by albumin-conjugated gold NPs[39–42] and nuclear damage by harming the de novo RNA biosynthesis.[43] Further studies are needed to gain a better understanding of the mechanism of NP-based photothermal therapy.

Most cancer therapeutic strategies target a tumor's microenvironment, such as inflammatory tumor-associated macrophages and cancer-associated fibroblasts, as they are considered to be key players in promoting tumorigenesis.[21] It has been published that inflammatory tumor-associated macrophages and cancer-associated fibroblasts have high uptake toward gold NPs.[44–46] Our results showed complete clearance of

the tumor with no relapse or metastasis. Therefore, we expect that PPTT has a significant effect on a tumor's microenvironment, which is most likely related to the high uptake of AuNRs and therefore consistent with the higher photothermal response for cancer-associated fibroblasts and inflammatory tumor-associated macrophages in the tumor microenvironment.[47–48] Further studies will be conducted to examine the effect of AuNRs-PPTT on changing a tumor's microenvironment.

Conclusion

We developed a three PPTT treatment regime with 2-week intervals to gradually suppress the natural tumors of dogs and cats without causing any burning of the tumor or affecting the nearby healthy cells. The results show a complete tumor regression in the seven animals (13 tumors). Furthermore, 1 year after the completion of treatment, no signs of relapse or effects of toxicity were observed. This evidence shows not only the efficacy of AuNRs-PPTT as a proposed treatment, but also its viability as a safer alternative to conventional treatments. All animals were subjected to AuNRs-PPTT and showed no relapse or toxicity effect even 1 year after treatment.

Disclosure

The authors report no conflicts of interest in this work.

References

1. Huang XH, El-Sayed IH, El-Sayed MA. Applications of gold nanorods for cancer imaging and photothermal therapy. In: Grobmyer SR, Moudgil BM, editors. *Cancer Nanotechnology: Methods and Protocols*. Totowa, NJ: Humana Press Inc; 2010:343–357.
2. Maeda H, Wu J, Sawa T, Matsumura Y, Hori K. Tumor vascular permeability and the EPR effect in macromolecular therapeutics: a review. *J Control Release*. 2000;65(1–2):271–284.
3. Li WQ, Sun CY, Wang F, et al. Achieving a new controllable male contraception by the photothermal effect of gold nanorods. *Nano Lett*. 2013;13(6):2477–2484.

4. Liu X, Chen Y, Li H, et al. Enhanced retention and cellular uptake of nanoparticles in tumors by controlling their aggregation behavior. *ACS Nano*. 2013;7(7):6244–6257.

5. Duan X, Li Y. Physicochemical characteristics of nanoparticles affect circulation, biodistribution, cellular internalization, and trafficking. *Small*. 2013;9(9–10):1521–1532.

6. Mackey MA, Saira F, Mahmoud MA, El-Sayed MA. Inducing cancer cell death by targeting its nucleus: solid gold nanospheres versus hollow gold nanocages. *Bioconjug Chem*. 2013;24(6):897–906.

7. Dreaden EC, Mackey MA, Huang X, Kang B, El-Sayed MA. Beating cancer in multiple ways using nanogold. *Chem Soc Rev*. 2011;40: 3391–3404.

8. Bagley AF, Hill S, Rogers GS, Bhatia SN. Plasmonic photothermal heating of intraperitoneal tumors through the use of an implanted near-infrared source. *ACS nano*. 2013;7(9):8089–8097.

9. Bardhan R, Lal S, Joshi A, Halas NJ. Theranostic nanoshells: from probe design to imaging and treatment of cancer. *Acc Chem Res*. 2011;44(10): 936–946.

10. Ali MRK, Panikkanvalappil SR, El-Sayed MA. Enhancing the efficiency of gold nanoparticles treatment of cancer by increasing their rate of endocytosis and cell accumulation using rifampicin. *J Am Chem Soc*. 2014;136(12):4464–4467.

11. Hang ZJ, Wang J, Nie X, et al. Near infrared laser-induced targeted cancer therapy using thermoresponsive polymer encapsulated gold nanorods. *Journal of the American Chemical Society*. 2014;136: 7317–7326.

12. Ghtedari M, Oraevsky A, Copland JA, Kotov NA, Conjusteau A, Motamedi M. High sensitivity of in vivo detection of gold nanorods using a laser optoacoustic imaging system. *Nano Letters*. 2007;7:1914–1918.

13. Jang B, Park JY, Tung CH, Kim IH, Choi Y. Gold nanorod-photosensitizer complex for near-infrared fluorescence imaging and photodynamic/photothermal therapy in vivo. *Acs Nano*. 2011;5:1086–1094.

14. Ratto F, Matteini P, Rossi F, et al. Photothermal effects in connective tissues mediated by laser-activated gold nanorods. *Nanomedicine-Nanotechnology Biology and Medicine*. 2009;5:143–151.

15. Dickerson EB, Dreaden EC, et al. Gold nanorod assisted near-infrared plasmonic photothermal therapy (PPTT) of squamous cell carcinoma in mice. *Cancer Lett*. 2008;269(1):57–66.

16. Goodrich GP, Bao LL, Gill-Sharp K, Sang KL, Wang J, Payne JD. Photothermal therapy in a murine colon cancer model using near-infrared absorbing gold nanorods. *J Biomed Opt*. 2010;15(1): 018001.

17. Li ZM, Huang P, Zhang XJ, et al. RGD-conjugated dendrimer-modified gold nanorods for in vivo tumor targeting and photothermal therapy. *Molecular Pharmaceutics*. 2010;7:94–104.

18. Niidome T, Akiyama Y, Shimoda K, et al. In vivo monitoring of intravenously injected gold nanorods using near-infrared light. *Small*. 2008;4:1001–1007.

19. Niidome T, Akiyama Y, Yamagata M, et al. Poly(ethylene glycol)-modified gold nanorods as a photothermal nanodevice for hyperthermia. *Journal of Biomaterials Science-Polymer Edition*. 2009; 20:1203–1215.

20. Pattani VP, Shah J, Atalis A, Sharma A, Tunnell JW. Role of apoptosis and necrosis in cell death induced by nanoparticle-mediated photothermal therapy. *J Nanoparticle Res*. 2015;17(1):11.

21. Song AS, Najjar AM, Diller KR. Thermally induced apoptosis, necrosis, and heat shock protein expression in 3D culture. *J Biomech Eng*. 2014;136(7).

22. Perez-Hernandez M, del Pino P, Mitchell SG, et al. Dissecting the molecular mechanism of apoptosis during photothermal therapy using gold nanoprisms. *ACS Nano*. 2015;9(1):52–61.

23. Shafiee R, Javanbakht J, Atyabi N, et al. Diagnosis, classification and grading of canine mammary tumours as a model to study human breast cancer: an Clinico-Cytohistopathological study with environmental factors influencing public health and medicine. *Cancer Cell Int*. 2013;13:79.

24. Shafiee R, Javanbakht J, Atyabi N, et al. Comparative value of clinical, cytological, and histopathological features in feline mammary gland tumors; an experimental model for the study of human breast cancer. *Diagn Pathol*. 2013;8:136.

25. Manesh JY, Shafiee R, Pedram B, et al. Improving the diagnosis, treatment, and biology patterns of feline mammary intraepithelial lesions: a potential model for human breast masses with evidence from epidemiologic and cytohistopathologic studies. *Tumour Biol*. 2014; 35(12):12109–12117.

26. Yu M, Guo F, Tan F, Li N. Dual-targeting nanocarrier system based on thermosensitive liposomes and gold nanorods for cancer thermo-chemotherapy. *J Control Release*. 2015;215:91–100.

27. Zhou T, Yu MF, Zhang B, et al. Inhibition of cancer cell migration by gold nanorods: molecular mechanisms and implications for cancer therapy. *Advanced Functional Materials*. 2014;24(44):6922–6932.

28. Ali MRK, Snyder B, El-Sayed MA. Synthesis and optical properties of small Au nanorods using a seedless growth technique. *Langmuir*. 2012;28(25):9807–9815.

29. Ellman GL. Tissue sulfhydryl groups. *Arch Biochem Biophys*. 1959; 82(1):70–77.

30. Ali MRK, Ali HR, Rankin CR, El-Sayed MA. Targeting heat shock protein 70 using gold nanorods enhances cancer cell apoptosis in low dose plasmonic photothermal therapy. *Biomaterials*. 2016; 102:1–8.

31. Mackey MA, Ali MRK, Austin LA, Near RD, El-Sayed MA. The most effective gold nanorod size for plasmonic photothermal therapy: theory and in vitro experiments. *J Phys Chem B*. 2014;118(5): 1319–1326.

32. Oldenburg SJ, Averitt RD, Westcott SL, Halas NJ. Nanoengineering of optical resonances. *Chem Physics Lett*. 1998;288(2–4): 243–247.

33. Sapareto SA, Dewey WC. Thermal dose determination in cancer therapy. *Int J Radiat Oncol Biol Phys*. 1984;10(6):787–800.

34. Yang L, Tseng Y-T, Suo G, et al. Photothermal therapeutic response of cancer cells to aptamer–gold nanoparticle-hybridized graphene oxide under NIR illumination. *ACS Appl Mater Interfaces*. 2015;7(9): 5097–5106.

35. Nam J, La W-G, Hwang S, et al. pH-responsive assembly of gold nano-particles and "spatiotemporally concerted" drug release for synergistic cancer therapy. *ACS Nano*. 2013;7(4):3388–3402.

36. von Maltzahn G, Park JH, Agrawal A, et al. Computationally guided photothermal tumor therapy using long-circulating gold nanorod antennas. *Cancer Res*. 2009;69(9):3892–3900.

37. Huang XH, Kang B, Qian W, et al. Comparative study of photothermo-lysis of cancer cells with nuclear-targeted or cytoplasm-targeted gold nanospheres: continuous wave or pulsed lasers. *J Biomed Opt*. 2010; 15(5):7.

38. Kang B, Austin LA, El-Sayed MA. Observing real-time molecular event dynamics of apoptosis in living cancer cells using nuclear-targeted plasmonically enhanced raman nanoprobes. *ACS Nano*. 2014; 8(5):4883–4892.

39. Zhang S, Li Y, He X, et al. Photothermolysis mediated by gold nanorods modified with EGFR monoclonal antibody induces Hep-2 cells apoptosis in vitro and in vivo. *Int J Nanomedicine*. 2014;9: 1931–1946.

40. Mocan L, Matea C, Tabaran FA, et al. Photothermal treatment of liver cancer with albumin conjugated gold nanoparticles initiates Golgi Apparatus-ER dysfunction and caspase-3 apoptotic pathway activation by selective targeting of Gp60 receptor. *Int J Nanomedicine*. 2015;10:5435–5445.

41. Cheng L, Yang K, Chen Q, Liu Z. Organic stealth nanoparticles for highly effective in vivo near-infrared photothermal therapy of cancer. *ACS Nano*. 2012;6(6):5605–5613.

42. Liu X, Tao H, Yang K, Zhang S, Lee ST, Liu Z. Optimization of surface chemistry on single-walled carbon nanotubes for in vivo photothermal ablation of tumors. *Biomaterials*. 2011;32(1):144–151.

43. Kodiha M, Hutter E, Boridy S, Juhas M, Maysinger D, Stochaj U. Gold nanoparticles induce nuclear damage in breast cancer cells, which is further amplified by hyperthermia. *Cell Mol Life Sci*. 2014; 71(21):4259–4273.

44. Ward C, Langdon SP, Mullen P, et al. New strategies for targeting the hypoxic tumour microenvironment in breast cancer. *Cancer Treat Rev*. 2013;39(2):171–179.

45. Luo YP, Zhou H, Krueger J, et al. Targeting tumor-associated macrophages as a novel strategy against breast cancer. *J Clin Invest*. 2006; 116(8):2132–2141.

46. Madsen SJ, Christie C, Hong SJ, et al. Nanoparticle-loaded macrophage-mediated photothermal therapy: potential for glioma treatment. *Lasers Med Sci*. 2015;30(4):1357–1365.

47. Costa EC, Gaspar VM, Marques JG, Coutinho P, Correia IJ. Evaluation of Nanoparticle uptake in co-culture cancer models. *PLoS One*. 2013;8(7):13.

48. Calvo F, Ege N, Grande-Garcia A, et al. Mechanotransduction and YAP-dependent matrix remodelling is required for the generation and maintenance of cancer-associated fibroblasts. *Nat Cell Biol*. 2013;15(6): 637–646.

Supplementary materials
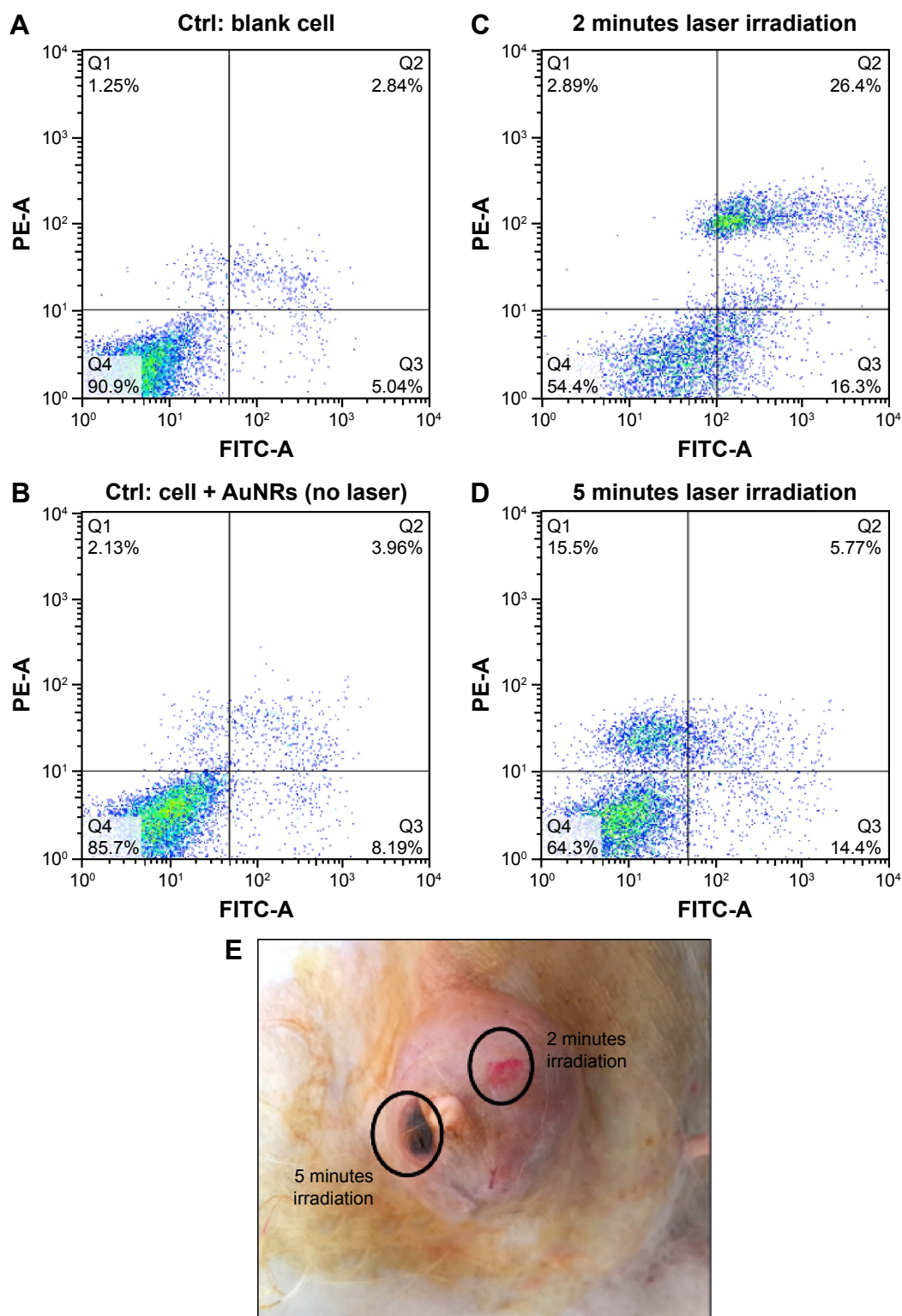
Figure S1 Modulation of PPTT toward inducing cancer cell apoptosis.
Notes: (**A–D**) Shows the MCF-7 cell apoptosis/necrosis states of the in vitro experiment. (**A**) Cells without AuNRs. (**B**) Cells incubated with AuNRs (no laser). (**C**) Cells incubated with AuNRs and 2 minutes laser irradiation. (**D**) Cells incubated with AuNRs and 5 minutes laser irradiation. (**E**) Laser irradiation spots of animals. The 5-minute irradiation caused burning of the tumor, whereas 2-minute irradiation shows no obvious change in appearance. The in vitro and in vivo experiments were conducted at the same condition.
Abbreviations: PPTT, plasmonic photothermal therapy; AuNRs, gold nanorods; ctrl, control.
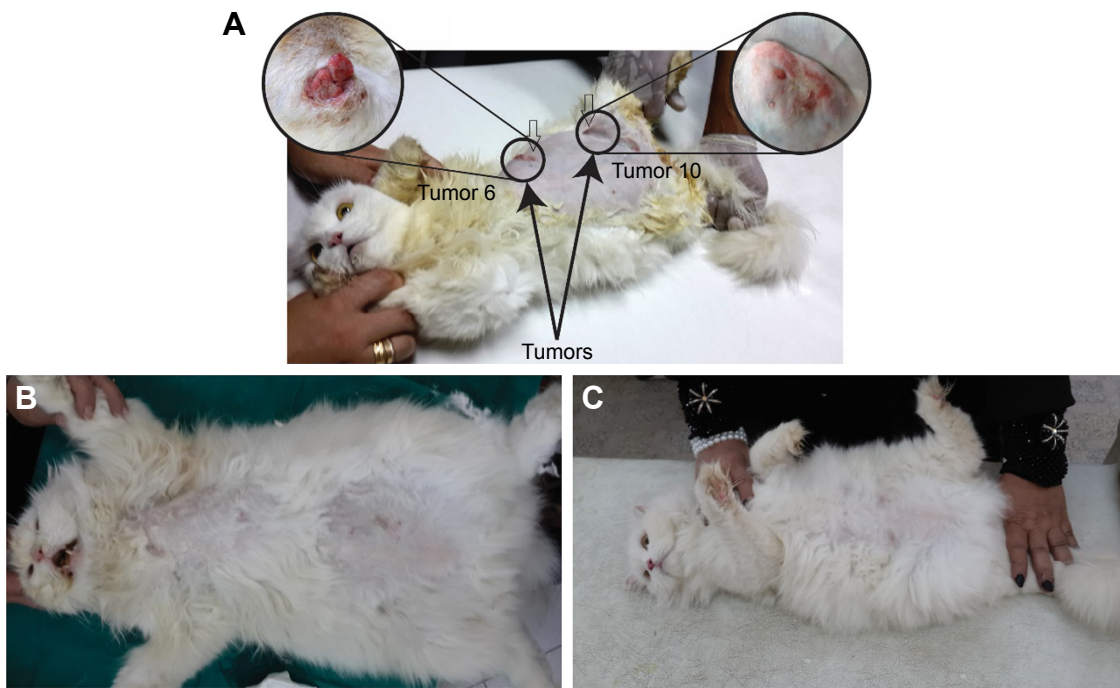
Figure S2 Photographs complete for Case 7 (Tumor 6: caudo-inguinal opened tumor and Tumor 10: anterior thoracic tumors) showing tumor regression after each treatment.
Note: (**A**) Before treatment, (**B**) 2 weeks after the third treatment, and (**C**) 1 year after the third treatment.
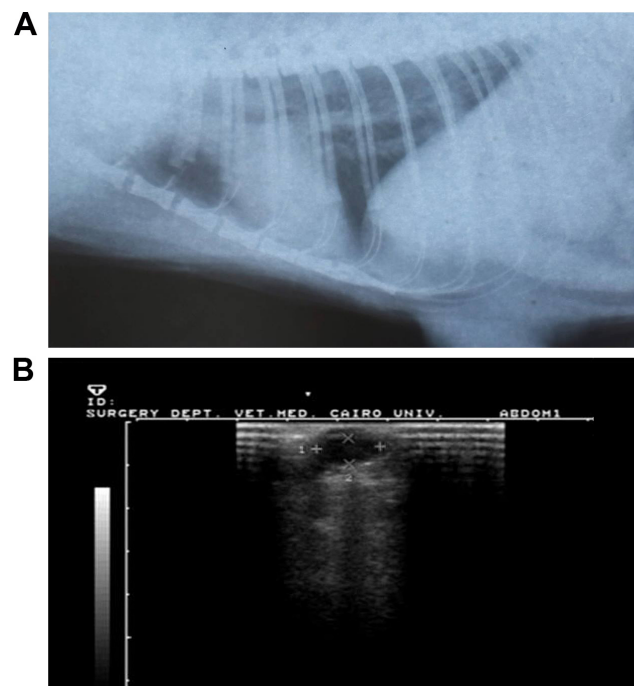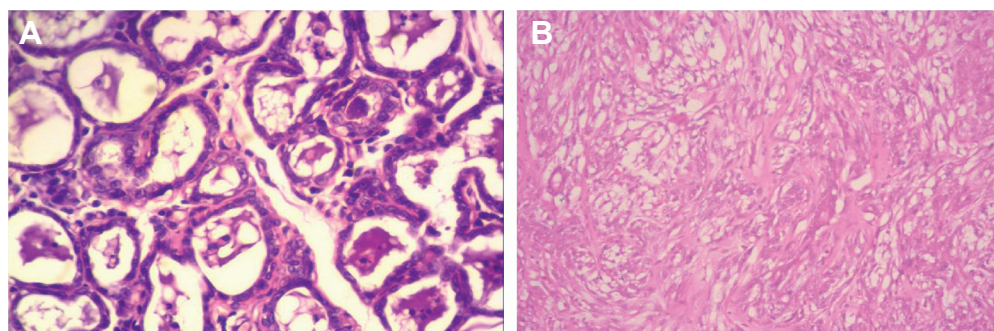

Figure S3 Case 2 before treatment.
Notes: (**A**) The X-ray shows there is no metastasis in the internal organs. (**B**) Ultrasound shows the tumor location, shape, and dimensions.
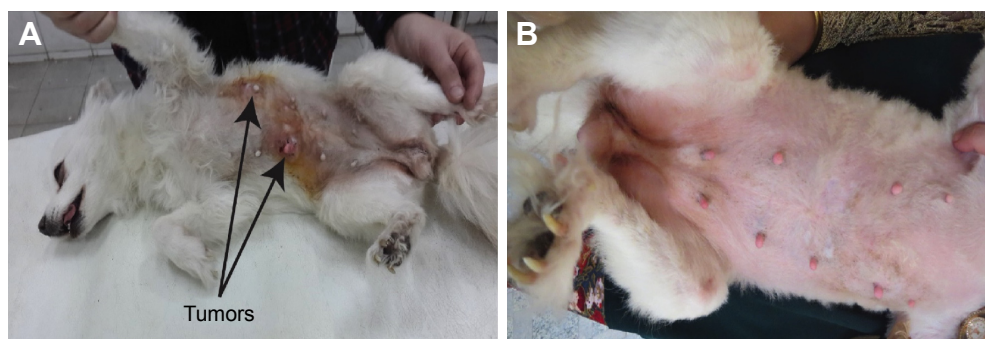
Figure S4 Photographs for Case 2 (Tumor 4: left caudothoracic mammary gland and Tumor 9: right abdominal mammary gland) showing the tumor regression 2 weeks after first treatment (**A**) and 1 year after the third treatment (**B**).
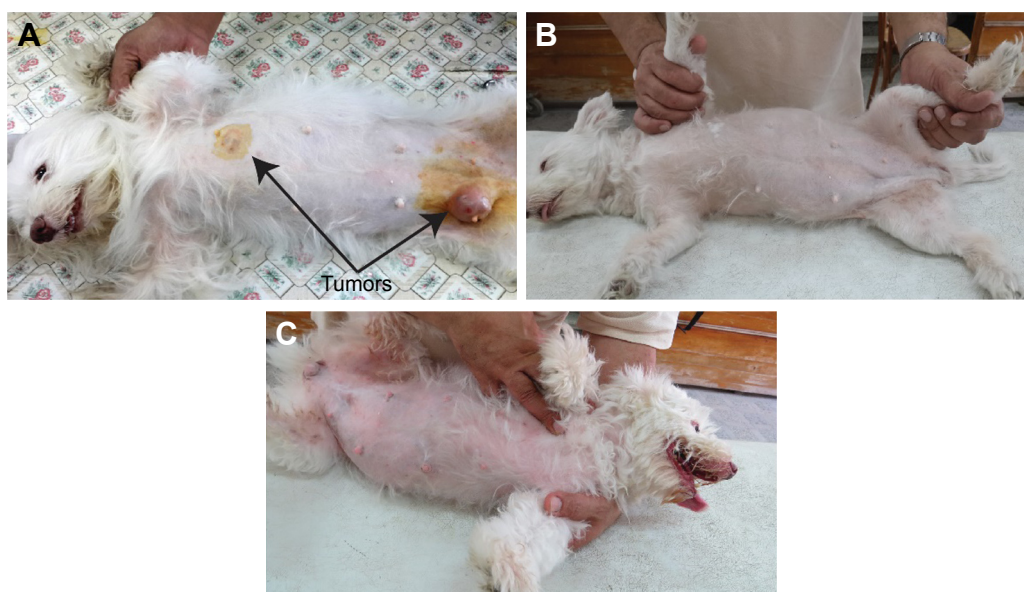
Figure S5 Photographs for case 3 (Tumor 2: left caudothoracic mammary gland and Tumor 13: right abdominal mammary gland) showing the tumor regression after each treatment.
Note: (**A**) Before treatment, (**B**) 2 weeks after the third treatment, and (**C**) 1 year after the third treatment.

Figure S6 Histopathology images (stained with H&E [×400]) for Case 3.
Notes: (**A**) Well-differentiated tubular adenocarcinoma before treatment. Carcinoma arranged in tubular pattern. Mass characterized by an intra-acinar deeply basophilic secretion and corpora amylecea. Connective tissue stroma infiltrated with mononuclear cells (tumor Grade III). (**B**) 2 weeks after the third treatment, there was absence of epithelial lining of acini and absence of acini and basement membrane. Also, loss of acinar pattern proliferation of fibrous connective stroma was seen (tumor Grade 0). Magnification of histopathology images stained with H&E: (**A**) ×200; (**B**) ×100.
Abbreviation: H&E, hematoxylin and eosin.
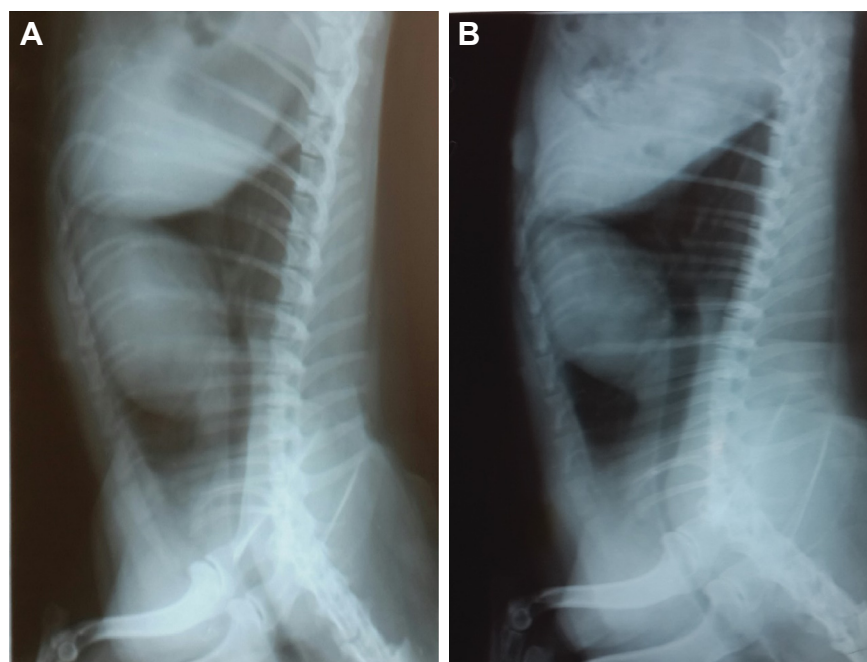
Figure S7 X-ray lateral exposure for Case 3 after treatment.
Note: (**A**) 2 weeks after third treatment, (**B**) 1 year after third treatment, showing there is no metastasis.